High-performance DUV AlGaN multi-quantum well LED with step-graded n-type AlInGaN electron blocking layer

SAMADRITA DAS[1], TRUPTI RANJAN LENKA[1,*], FAZAL AHMED TALUKDAR[1], GIOVANNI CRUPI[2],
HIEU PHAM TRUNG NGUYEN[3]

[1]*Department of Electronics and Communication Engineering, National Institute of Technology Silchar, Assam, 788010, India*
[2]*BIOMORF Department, University of Messina, Messina 98125, Italy*
[3]*Department of Electrical and Computer Engineering, Texas Tech University, 1012 Boston Avenue, Lubbock, Texas 79409, USA*

In this paper, we propose a novel deep ultra-violet (DUV) AlGaN/GaN multi-quantum well light-emitting diode (LED) with a step-graded n-type AlInGaN electron blocking layer (EBL) instead of a conventional p-type AlGaN EBL. This is designed for a~265 nm wavelength emission without affecting the hole injection efficiency. Due to enhanced carrier transport in the step-graded n-type EBL structure, there occurs reduced electron leakage into the p-region, superior hole activation and hole injection, improved output power and internal quantum efficiency (IQE). Moreover, this specially designed EBL reduces the quantum confined stark effect in the active region, ultimately enhancing the carrier wave functions overlap. The device structure is simulated using Atlas technology computer-aided design (TCAD). The internal quantum efficiency is improved from ~36.48% to ~49.46% while switching from conventional p-type EBL to step-graded n-type EBL. Furthermore, our proposed structure exhibits 1.61% efficiency droop, which is significantly ~4.8 times lower as compared to the regular structure.

1. Introduction

Due to the wide band-gap, aluminium gallium nitride (AlGaN) based deep ultra-violet (DUV) light-emitting diodes (LED) are capable of replacing the existing incandescent UV light sources for a wide range of applications, such as water purification, pharmaceutical applications, and disinfection[1]–[4]. Across the entire UV-A, UV-B, and UV-C spectral range, UV LEDs offer significantly decreased power consumption, low cost, and reduced space[5]–[9].

Optical power and internal quantum efficiency (IQE) are considered to be the critical parameters, which need further improvement so that high-power LEDs can penetrate into the consumer industry of lighting[5], [6], [10]. However it gets hindered by the electron overflow into the p-GaN region and the inadequate hole supply into the active region[11][12]. Therefore to restrict this overflow, a p-type electron blocking layer (EBL) is inserted between the active region and p-GaN layers. The electrons are thus confined within the multi-quantum well (MQW) because of the huge potential barrier created by AlGaN layer, resulting in a low electron overflow. Because of the large defect density and dislocation in the active region, it is still difficult to obtain efficient p-type conduction in large Al content EBL[13]–[16]. This occurs due to various reasons related with magnesium (Mg)-dopants including tremendously large activation energy (till ~600 meV), little tendency to get soluble and self-

compensation while forming point defects[17], [18]. Because of in-effective Mg-doping, a very poor hole concentration occurs in this Al rich EBL[19]–[21]. In wide band-gap LEDs, inclusion of a large Al composition AlGaN layer critically compromises the hole injection. This happens as there is a large valence band offset in the hetero-interface which leads to rise in device resistivity, undesirable heating effect and decreased efficiency[22]. Also when the potential barrier height difference is large, it obstructs the hole transportation into the MQWs leading to insufficient hole supply taking part in the radiative recombination with electrons[23]. Therefore in an attempt to minimize electron overflow without compromising the hole injection, a novel LED structure has been proposed in this paper using step-graded n-type AlInGaN EBL inserted between the active region and n-AlGaN cladding layer. This EBL consists of silicon (Si)-doped AlInGaN permitting effective cooling of hot electrons before they inject into the active region and thus there is a less overflow of electrons. This also contributes to a lower turn on voltage for the n-type EBL. To address some of the above-mentioned issues, extensive studies have been done in the LED design structure perspective and optical performances have been developed with reduced dislocation density [24]–[28].

In our proposed device, due to step-graded EBL structure, the kinetic energy and electron velocity inserting the active region decrease which in turn reduce the

electron mean free path and improve the electron confinement in the EBL[29][30].

This paper is structured as follows: Section II is dedicated to a brief description of the simulation methodology, Section III is devoted to the presentation of the device structure and parameters, Section IV is focused on the presentation and discussion of the obtained results, and, finally, the conclusions are given in the last section.

2. Simulation methodology

In this work, the electrical and optical properties of the device structure are minutely simulated and studied with the help of commercially available industry standard Silvaco Atlas technology computer-aided design (TCAD) [31]. The device structure is described by a certain set of codes written in the Deck Build tool. The specific parameters such as length, width, doping concentration, and operating temperature are provided as the inputs. During the simulation process Shockley Read–Hall (SRH), Radiative and Auger recombination models are used. During the numerical simulations the Poisson, Continuity, and Schrodinger equations with appropriate boundary conditions are self-consistently solved using the Silvaco TCAD.

3. Device structure and parameters

Firstly, in order to validate our device model, we have examined the conventional AlGaN deep UV LED formed on a c-plane AlN template with ~284 nm emission wavelength as our reference device and denoted as LED$_1$ (see Fig. 1(a)). This work was studied and experimentally presented by Yan et al.[32]. LED$_1$ comprises of 3 µm n-Al$_{0.6}$Ga$_{0.4}$N layer (Si doping: 6×10^{18} cm^{-3}), followed by an active region, p-Al$_{0.65}$Ga$_{0.35}$N EBL (20 nm, Mg doping: 2×10^{19} cm^{-3}) and then capped by a 50 nm p-Al$_{0.5}$Ga$_{0.5}$N hole injection layer (Mg doping: 2×10^{19} cm^{-3}), and on the top a 80 nm p-GaN contact layer (Mg doping: 1×10^{20} cm^{-3}). The active region comprises of five intrinsic Al$_{0.4}$Ga$_{0.6}$N quantum wells (QWs of 3 nm) stuffed between six intrinsic Al$_{0.5}$Ga$_{0.5}$N quantum barriers (QBs of 12 nm). As illustrated in Fig. 1(c), the proposed device (LED$_2$) has the similar structure as LED$_1$ except that the uniform p-type AlGaN EBL is now replaced by step-graded n-type AlInGaN EBL prior to the active region. The LED chip has an overall area of 300 µm×300 µm which is operated under a temperature of 300 K and the internal absorption loss is assumed as 2000 m^{-1}.

The benefit of n-type EBL consisting of AlInGaN step-graded layers is the effective cooling of hot electrons

before injecting in the active region and thus minimizing overflow of electrons. Also due to the absence of any potential barrier, effective injection of holes can be achieved into the active region. Because of minimized reduced barrier to hole injection, a lower turn-on voltage for n-type EBL is obtained. The EBL of LED$_2$ is divided into five layers of Al$_x$In$_y$Ga$_z$N; each has a thickness of 4 nm. This layer is uniformly step-graded in such a way that the constituent values of x, y, z is (0.8, 0.03, 0.17), followed by step-wise reduction of Al composition by 10% and 10% increase of gallium composition in each layer (0.7, 0.03, 0.27 for next layer) and so on up to five consecutive divisions till (0.4, 0.03, 0.57) in the last layer. The proposed device (LED$_2$) is reformed from LED$_1$ by changing a few layers and the doping type of EBL. The constituents in the new layer are estimated and then decided in order to get a wavelength range of 250-285 nm.

The energy band-gap of GaN and AlGaN are calculated with the help of Varshni formula[33]:

$$E_g(T_L) = E_g(0\,K) - \frac{\alpha T_L^2}{T_L + \beta} \tag{1}$$

where $E_g(T_L)$ and $E_g(0K)$ are energy band-gap at T_L and 0K temperature, respectively; while α and β are known as material constants. The respective values of α, β, and $E_g(0K)$ are 0.909 meV/K, 830 K and 3.507 eV for GaN and 1.799 meV/K, 1462 K and 6.23 eV for AlN[33].

The energy band-gap of Al$_m$Ga$_{1-m}$N is calculated using the following equation:

$$E = m.E^{AlN} + (1-m).E^{GaN} - b.m.(1-m) \tag{2}$$

where b=0.94 is the bowing parameter, band-offset ratio is taken as 0.67/0.33[34]. The band-gap of GaN and AlN are taken as 3.42 eV and 6.2 eV, respectively[35]. The Auger recombination, radiative recombination, SRH recombination coefficient, and light extraction efficiency are taken as 2.88×10^{-30} cm^6/s, 2.13×10^{-11} cm^3/s, 6.67×10^7/s, and 15%, respectively[36], [37]. Also, the Mg activation energy is scaled linearly from 170 meV to 510 meV for p-$Al_xGa_{1-x}N$ alloy[38]. The electron and hole mobilities are estimated by Cauchy-Thomas approximation[39] and band energy diagrams are measured by using $6\times6\,k.p$ model[40]. Moreover, the degree of spontaneous and piezoelectric polarization is assumed to be 50% of the theoretical value and is estimated using the techniques of Fiorentini et al.[41]. The remaining parameters used in the simulation can be found elsewhere[42][43].
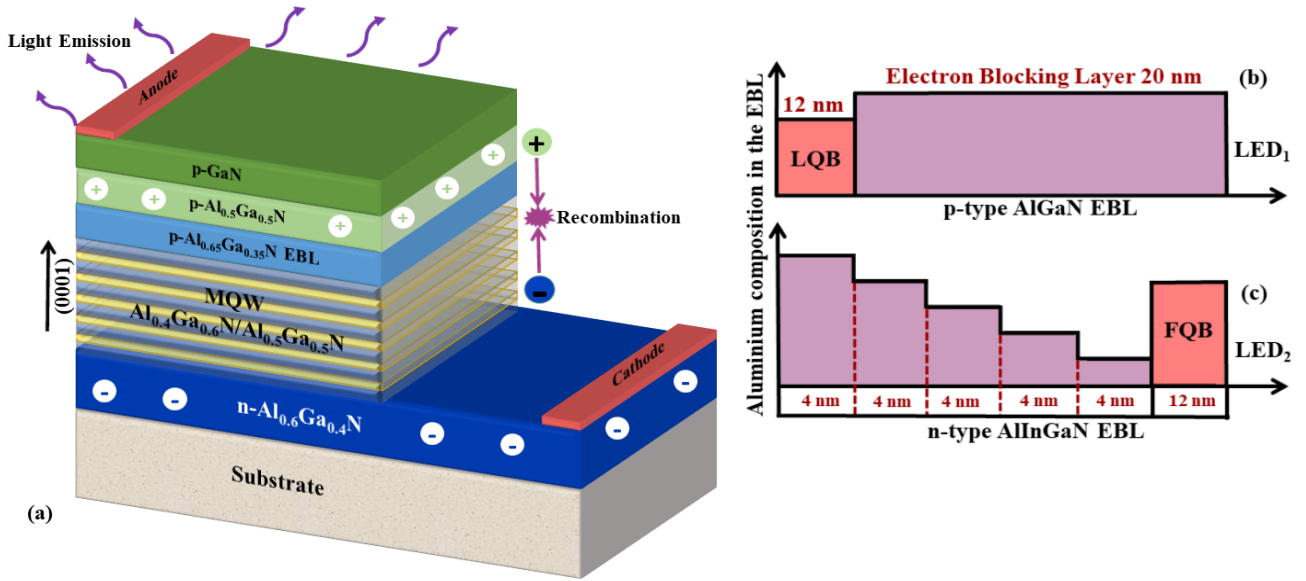
Fig. 1. (a) Schematic diagram of the conventional LED (LED₁). Al composition (%) profile related to the conduction band of (b) LED₁ with conventional p-type AlGaN EBL and of (c) LED₂ with step graded n-type AlInGaN EBL with uniformly decreasing Al composition. LQB and FQB represent last quantum barrier and first quantum barrier, respectively (color online)

4. Results and discussion

The device model and parameters which are numerically implemented in our work are optimized using the experimentally obtained data of reference structure i.e., LED₁. Fig. 2 shows that the numerically obtained results of power-current-voltage curves of LED₁ nearly match with the experimentally obtained graphs which validate the reliability of our device model. The parameters used in the experimental process of the device (mentioned in [32]) are used in this paper while designing LED₁ and the simulation process is undergone for calibration purpose After that, the simulated results of LED₁ and LED₂ are compared with the help of Silvaco Atlas.
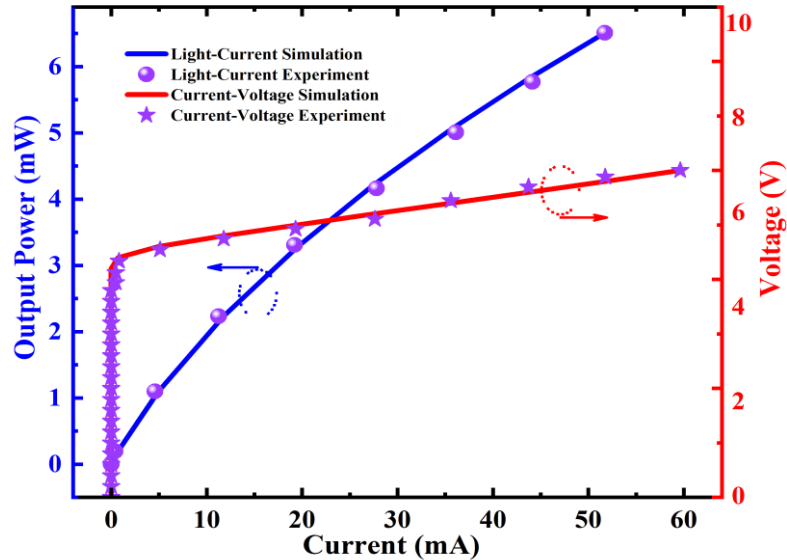

Fig. 2. Measured and calculated light-current-voltage characteristics of LED₁ for model validation (color online)

To investigate the performance of the proposed structure, the electroluminescence (EL) spectra of the designed LEDs are displayed in Fig. 3(a) at an injection current of 40 mA. The light intensity of LED₂ (peak wavelength ~276.5 nm) is stronger as compared to LED₁ (peak wavelength ~278.3 nm). However, the approximate wavelength ~284 nm is the fabricated result obtained by experimental method as mentioned in the paper [32]. But when the same device is simulated with Silvaco Atlas, the values obtain (~278.3 nm) nearly match with the previously acquired experimental results (~284 nm). The presence of a shoulder at ~280.5 nm other than the main peak at ~278.3 nm for LED₁ is due to significant electron overflow and the resulting parasitic emission from p-

AlGaN layer. Due to decrease in peak wavelength of LED$_2$, a very minute blue-shift is observed which is apparently assigned to the minimization of quantum-confined stark effect (QCSE) in our final structure. Additionally we have analysed the emission spectrum characteristics at various temperatures to differentiate the piezoelectric field (PZ) for the developed LEDs. In relation to the injection current, Figs. 3(b) and 3(c) display the LED$_1$ and LED$_2$ peak emission wavelengths at various ambient temperatures. According to Varshni eq (1), when temperature rises, the energy band gap gets narrowed, shifting the overall emission wavelength to a higher value.

This explains why, as temperature rises, the overall emission wavelength in Figs. 3(b) and 3(c) moves to a higher value. The blue-shift, caused by the band-filling effect and screening effect, induces the wavelength to initially shift towards a lesser value as the current rises [44]. But when the current continues to rise further, the wavelength moves to a longer value known as red-shift. This is because parasitic resistances have a thermal impact. From the dotted line extracted from Figs. 3(b) and 3(c), it is obvious that LED$_2$ has almost negligible blue-shift indicating a decrease in PZ of LED$_2$.
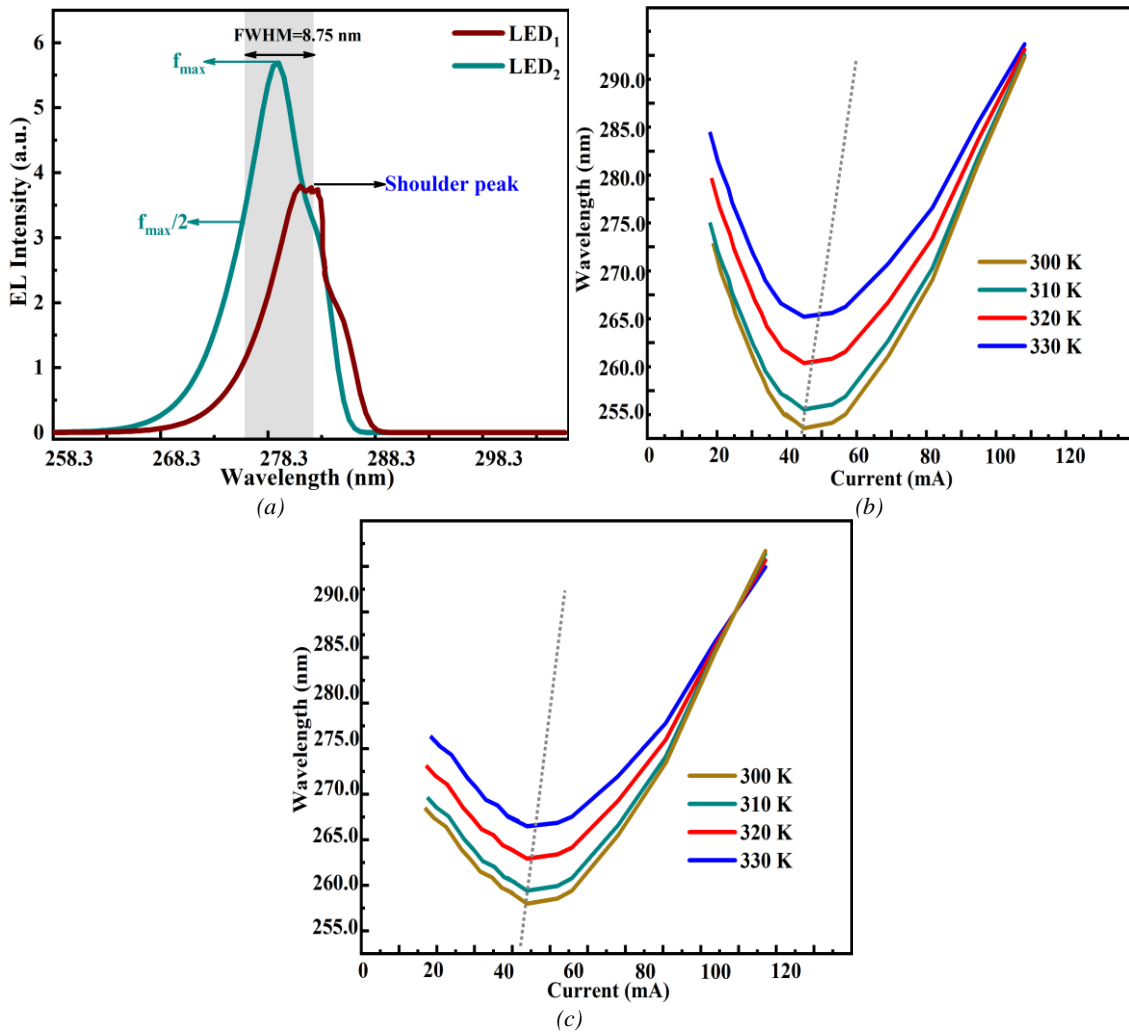

Fig. 3. (a) Electroluminescence (EL) intensity of LED$_1$ and LED$_2$ at an injection current of 40 mA, (b) Emission wavelengths as a function of injection current for LED$_1$ and (c) LED$_2$ (color online)

In order to understand the underlying mechanism, the energy band diagram and the quasi-Fermi level of the simulated structures are analysed at 40 mA current in Figs. 4(a) and 4(b). The effective conduction band barrier height CBBH (Φ_C) at each barrier (n) and EBL (Φ_{EBL}) of LED$_2$ is comparatively higher than LED$_1$ as listed in Table 1. The higher and progressively improved Φ_C in LED$_2$ constructively confines the electrons in the active region and resists the electron overflow into the p-region. From Fig. 4(a) the p-type EBL generates an energy barrier

height of 169.4 meV for holes. On the contrary, in Fig. 4(b), the n-type AlInGaN builds up an energy barrier of 90 meV for electrons before they enter the MQWs active region. Meanwhile, the n-EBL presents no blocking effect on the hole transport path into the QWs due to the absence of energy barrier. This leads to the reduction of non-radiative recombination in p-region and improves hole injection into the active region. Due to low strain and lattice mismatch between the epi-layers, the effective

CBBH alleviates and suppresses electron leakage; keeping the hole transportation intact.
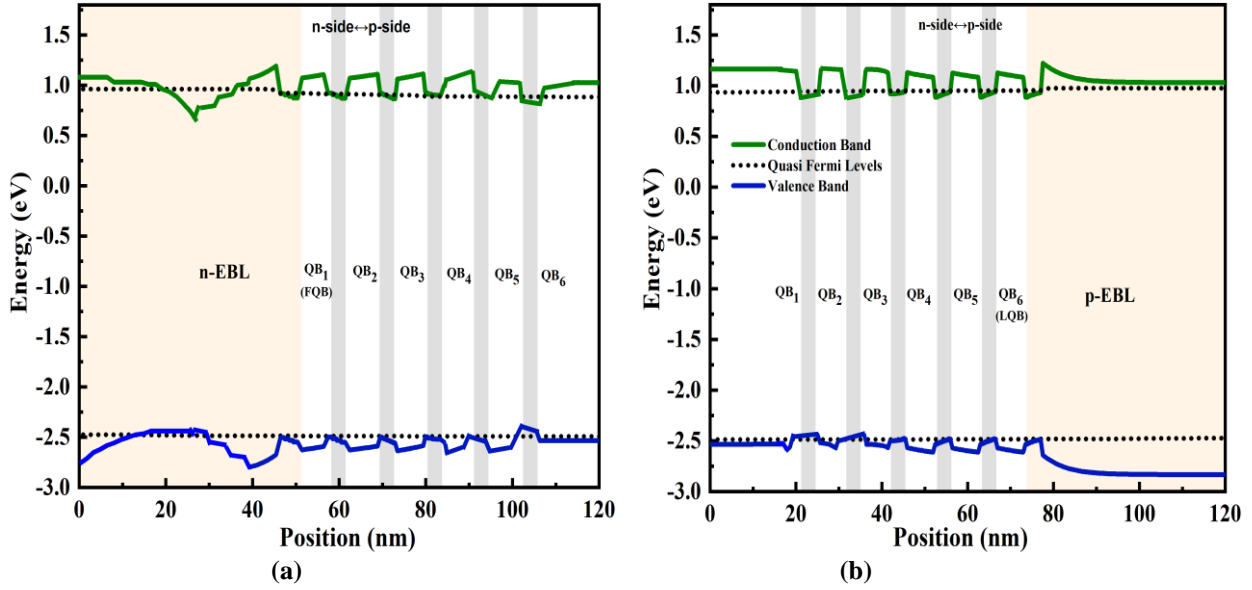

Fig. 4. Energy band profile of (a) the conventional LED (LED₁) and of (b) the proposed LED with step-graded n-type EBL (LED₂) at 40 mA (color online)

Table 1. Effective CBBH (Φ_{en}), VBBH (Φ_{hn}) of QBs and EBL (Φ_{EBL}) for LED₁ and LED₂ (in meV)

CBBH	LED₁	LED₂	VBBH	LED₁	LED₂
Φ_{e2}	107.8	197.1	Φ_{h2}	72.9	75.9
Φ_{e3}	159.1	203.7	Φ_{h3}	76.8	80.8
Φ_{e4}	180.4	312.7	Φ_{h4}	72.2	84.6
Φ_{e5}	176.6	367	Φ_{h5}	81.6	86.2
Φ_{e6}	174.7	343.9	Φ_{h6}	80.3	107.1
Φ_{EBL}	255.46	368.04			

Due to the aforesaid reasons, an improved carrier concentration in LED₂ at 40 mA injection current is observed as shown in Fig. 5(a), where the electron concentration of LED₂ is increased by 51.1% (for reference, the third QW is considered). For the device with p-type EBL (LED₁), electron concentration is not uniformly distributed and is much higher in the first and the last QWs. However, for the device with the n-AlInGaN EBL electron distribution is much more uniform. Similarly from Fig. 5(b), the holes in the MQWs of LED₂ rise by 52.8%. Because of the enhanced carrier concentration, the electron leakage is minimized in LED₂ which encourages hole transport into the MQWs. The electron overflow into the p-GaN region is lower in LED₂ as it has less electron concentration in the p-GaN region which is evident from

electron leakage density curves in Fig. 5(c). Hence, the electron blocking effect of the n-AlInGaN EBL is found to be more effective than p-EBL.

In LED₂ electrons need to overcome a higher CBBH to reach the p-layer. Because of this, non-radiative recombination of leaked electrons within the holes in the p-side is lowered and availability of holes to be injected towards the active region is more. Consequently a better radiative recombination rate is observed in LED₂, due to stronger carrier concentration, as displayed in Fig. 6. For clear visualization, the position of values in the x-axis is slightly shifted for the two samples. The electron-hole pair recombination for LED₂ is enormously improved by 93.3% than LED₁ (for reference, third QW is considered).
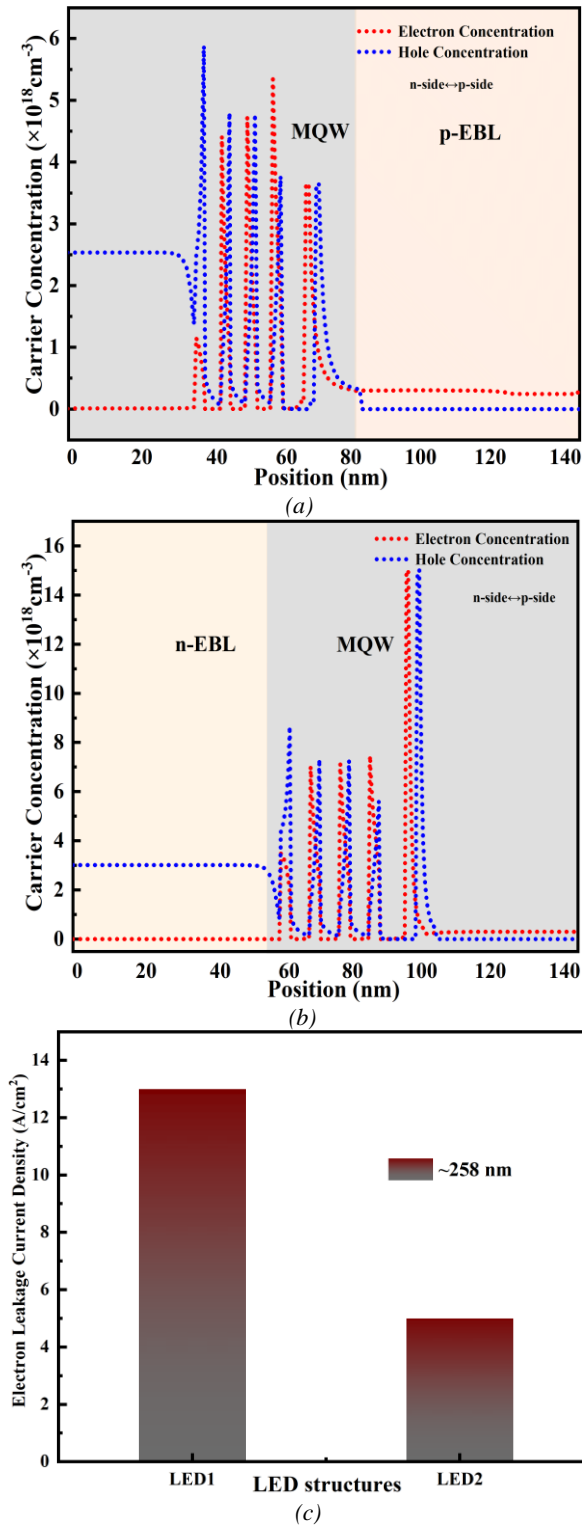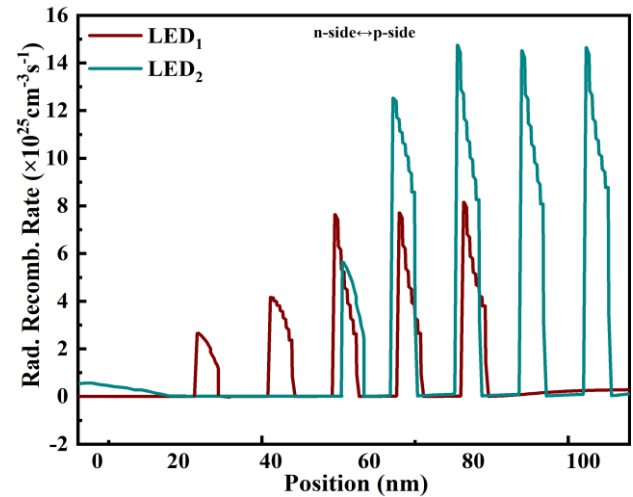
Fig. 6. Radiative recombination rate of both LED₁ and LED₂ at 40 mA (color online)

To understand the carrier transport improvement in the proposed structure (LED$_2$) we have studied their corresponding IQE and output power performance, as presented in Fig. 7. It is apparent that IQE is significantly higher for LED$_2$ with step-graded n-type EBL by 35.58% at a current injection of 40 mA. This indicates the detrimental impact of p-type EBL on hole injection. Interestingly, the efficiency droop defined as $(\eta_{peak} - \eta_{40 mA})/ \eta_{peak}$, is severely decreased up to ~1.61% in LED$_2$, while LED$_1$ exhibits ~9.42% droop at 40 mA current. This is due to the enhanced carrier transportation and confinement of carriers in the active region of LED$_2$. The amelioration in the IQE and decrease in droop in LED$_2$ are attributed to the improved radiative recombination and reduced carrier leakage, owing to superior carrier confinement [45]. This is provided by the step-graded n-type EBL. As shown in Fig. 8, the turn-on voltage of the two structures is nearly the same. However, it is inevitable that LED$_2$ exhibits a slightly higher operating bias voltage at 40 mA than LED$_1$ due to the presence of step graded n-type AlInGaN EBL.
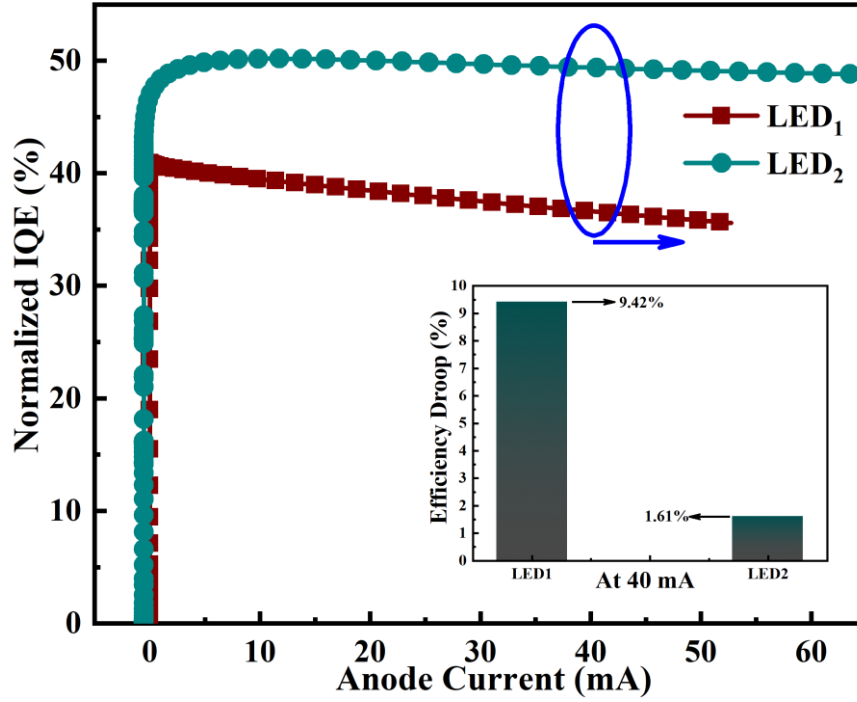

Fig. 5. Carrier concentration in the MQWs of (a) the conventional LED (LED₁) and of (b) the proposed LED (LED₂) at 40 mA; (c)Electron leakage current density of LED₁ and LED₂ (color online)

Fig. 7. IQE as a function of injected current in both LED₁ and LED₂. Inset: Efficiency droop for each LED at 40 mA (color online)
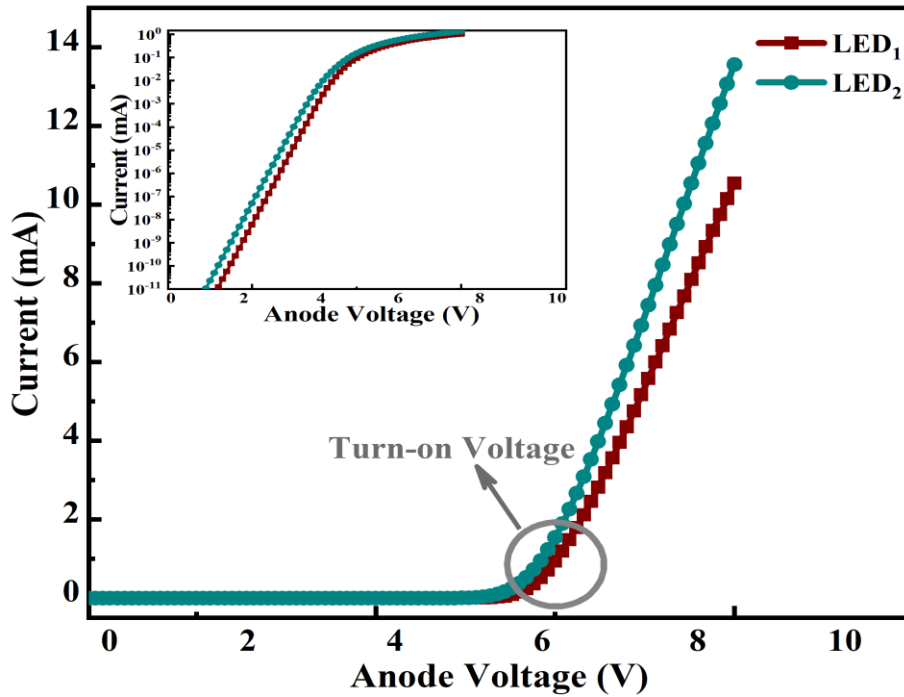

Fig. 8. I-V behaviour of both LED₁ and LED₂ in linear scales; Inset: Re-plotting of the I-V curves in a semi-log scale (color online)

From Fig. 9, LED₂ has a great enhancement of light output power throughout the whole current range while compared to LED₁. LED₂ exhibits an optical power of ~6.91 mW at 40 mA, which is almost 30.1% times higher than that measured for LED₁ with p-EBL. This improvement in light power indicates that more carriers radioactively recombine in QW of LED₂. In order to have better understanding of the physical mechanism of enhanced carrier confinement in our proposed structure,

the electrostatic field at 40 mA injection current in the active region is studied mathematically and displayed in Fig. 10. Using Eqs. (3)-(5), the electrostatic field can be estimated as follows [46]:

$$E_{QB} \approx \frac{t_{EBL} \times \Delta P(w)}{t_{EBL} \times \varepsilon_{QB} + t_{QB} \times \varepsilon_{EBL}} \tag{3}$$

$$E_{QB} \times t_{QB} = E_{QW} \times t_{QW} \qquad (4)$$

$$\Delta P(w) = \sigma_s^{Pol}\big|(w = 0) - \rho_{QB}^{Pol} \times w\big|(w < t_{QB}) \quad (5)$$

where E_{QB} and E_{QW} are electrostatic field in QB and QW, respectively, $\Delta P(w)$ represents net polarization charge density along the growth direction 'w', ε_{QB} and ε_{EBL} represent di-electric constants of QB and EBL respectively, t_{QB} and t_{EBL} are the width of QB and EBL, respectively, σ_s^{Pol} is the polarization-induced sheet charge density, and ρ_{QB}^{Pol} represents the polarization-induced bulk charge density. Lower electrostatic field in the QW confines electrons and holes more effectively and eventually improves the radiative recombination which leads to better efficiency. Eq. 4 depicts that E_{QB} is directly

proportional to E_{QW}. Also from Eq. 3, E_{QB} can be decreased by reducing the value of $\Delta P(w)$ which is eventually connected to σ_s^{Pol} and ρ_{QB}^{Pol} as depicted in Eq.5. σ_s^{Pol} for LED$_2$ is comparatively lower than LED$_1$ due to reduced spontaneous polarization discontinuity at QB/EBL interface and suppressed piezoelectric polarization effect. Moreover, due to compositionally step-graded profile in LED$_2$, ρ_{QB}^{Pol} can be raised which will reduce $\Delta P(w)$ and ultimately E_{QB}. Furthermore in LED$_2$, the super-lattice EBL structure t_{EBL} is 4 nm due to the first step which is lower than LED$_1$ (t_{EBL} is 20 nm). This in turn again reduces the electrostatic field in the barrier/EBL interface for LED$_2$, also evident from Fig. 10. The output parameters of the different structures are provided in Table 2 for comparison.
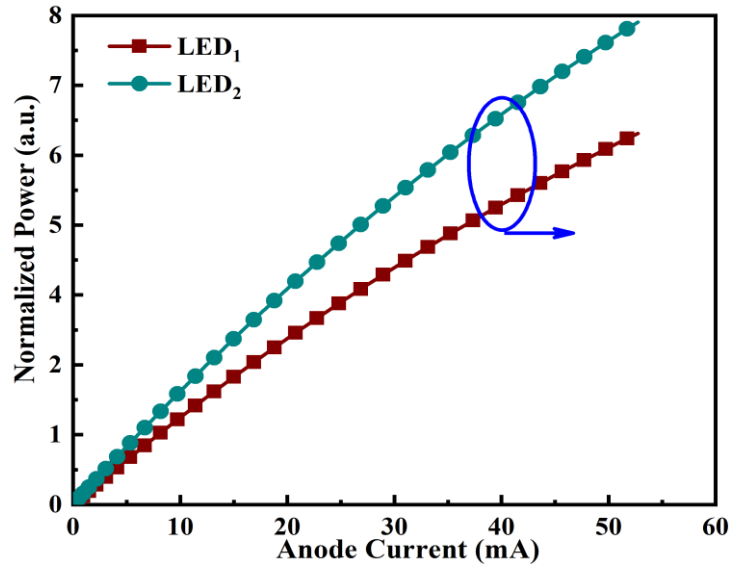

Fig. 9. Output power of both LED$_1$ and LED$_2$ as a function of injection current (color online)
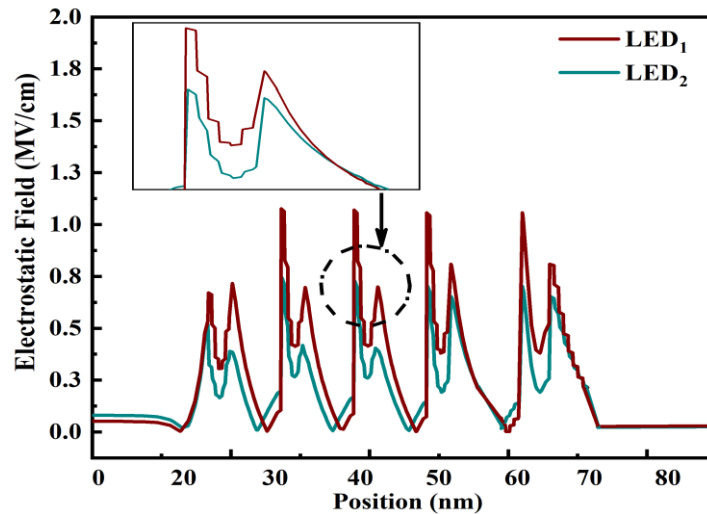

Fig. 10. Magnitude of electrostatic field in the active region of LED$_1$ and LED$_2$; Inset: Electrostatic field in the 3rd QW (color online)

Table 2. Optimized performance parameters of the conventional and proposed structures

Parameters	LED$_1$	LED$_2$
Electron Concentration at 3rd QW (cm^{-3})	4.72×10^{18}	7.13×10^{18}
Hole Concentration 3rd QW (cm^{-3})	4.78×10^{18}	7.26×10^{18}
IQE at 40 mA (%)	36.48	49.46
Efficiency Droop at 40 mA (%)	9.42	1.61
Power at 40 mA(mW)	5.32	6.91
Operating Bias Voltage at 40 mA(V)	7.01	7.42
Radiative Recombination Rate at 3rd QW(cm^{-3}s^{-1})	7.63×10^{25}	14.7×10^{25}

5. Conclusion

In conclusion, we have explored the impact of EBL on the output performance of AlGaN UV LEDs. From the achieved simulation results, it is evident that step-graded n-type AlInGaN EBL has better advantages compared to conventional p-type AlGaN EBL. It reduces electron overflow without compromising hole transport and hole injection into the active region, thereby having a better balance between hole and electron injection in the active region. Step-graded promotes the hole injection by forming negative sheet polarization charges and improves the spatial overlap of the electron-hole wave function. A significant improvement in both IQE (by 23.51%) and power (by 71.48%) of LED$_2$ is measured compared to LED$_1$. Also there is an increase of hole concentration, 8.65×10^{18} cm^{-3} in LED$_2$. Furthermore LED$_2$ is observed to have a minimal efficiency droop of 1.172% and lower electrostatic field. In the future, extended device performance is expected by optimizing the p-type doping which will further improve the light extraction efficiency along with minimized efficiency droop.

References

[1] K. Davitt, Y.-K. Song, W. R. Patterson III, A. V. Nurmikko, M. Gherasimova, J. Han, Y.-L. Pan, R. K. Chang, Opt. Express **13**(23), 9548 (2005).
[2] L. Kemény, Z. Csoma, E. Bagdi, A. H. Banham, L. Krenács, A. Koreck, Br. J. Dermatol. **163**(1), 167 (2010).
[3] P. J. Parbrook, T. Wang, IEEE J. Sel. Top. Quantum Electron. **17**(5), 1402 (2011).
[4] A. Khan, K. Balakrishnan, T. Katona, Nat. Photonics **2**(2), 77 (2008).
[5] H. Hirayama, N. Maeda, S. Fujikawa, S. Toyoda, N. Kamata, Jpn. J. Appl. Phys. **53**(10), 100209 (2014).
[6] H. Sun, T. D. Moustakas, Appl. Phys. Express **7**(1), 1 (2014).
[7] Y. Kashima, N. Maeda, E. Matsuura, M. Jo, T. Iwai, T. Morita, M. Kokubo, T. Tashiro, R. Kamimura,

Y. Osada, H. Takagi, H. Hirayama, Appl. Phys. Express **11**(1), 012101 (2018).
[8] M. Jo, N. Maeda, H. Hirayama, Appl. Phys. Express **9**(1), 7 (2016).
[9] S. Das, T. R. Lenka, F. A. Talukdar, R. T. Velpula, H. P. T. Nguyen, Opt. Quantum Electron. **55**(1), 101007 (2022).
[10] Samadrita Das, Trupti Ranjan Lenka, Fazal Ahmed Talukdar, Sharif Md. Sadaf, Ravi Teja Velpula, Hieu Pham Trung Nguyen, Appl. Opt. **61**(30), 8951 (2022).
[11] D. S. Shin, D. P. Han, J. Y. Oh, J. I. Shim, Appl. Phys. Lett. **100**(15), 153506 (2012).
[12] M. H. Kim, M. F. Schubert, Q. Dai, J. K. Kim, E. F. Schubert, J. Piprek, Y. Park, Appl. Phys. Lett. **91**(18), 1 (2007).
[13] T. D. Moustakas, MRS Commun. **6**(3), 247 (2016).
[14] S. I. Inoue, N. Tamari, M. Taniguchi, Appl. Phys. Lett. **110**(14), 141106 (2017).
[15] J. S. Speck, Mater. Sci. Forum **353-356**, 769 (2001).
[16] M. H. Chang, D. Das, P. V. Varde, M. Pecht, Microelectron. Reliab. **52**(5), 762 (2012).
[17] C. Stampfl, C. G. Van de Walle, Phys. Rev. B - Condens. Matter and Material Physics **65**(15), 1552121 (2002).
[18] X. Hua, Y. Guia, Y. Liua, L. Xua, L. Ranb, X. Chenc, Vacuum **193**(2), 110506 (2021).
[19] Y. H. Liang, E. Towe, Appl. Phys. Rev. **5**(1), 011107 (2018).
[20] K. Ebata, J. Nishinaka, Y. Taniyasu, K. Kumakura, Jpn. J. Appl. Phys. **57**(4), 4 (2018).
[21] Y. Chen, H. Wu, E. Han, G. Yue, Z. Chen, Z. Wu, G. Wang, H. Jiang, Appl. Phys. Lett. **106**(16), 162102 (2015).
[22] H. Hirayama, Y. Tsukada, T. Maeda, N. Kamata, Appl. Phys. Express **3**(3), 3 (2010).
[23] S. H. Han, D. Y. Lee, S. J. Lee, C. Y. Cho, M. K. Kwon, S. P. Lee, D. Y. Noh, D. J. Kim, Y. C. Kim, S. J. Park, Appl. Phys. Lett. **94**(23), 1 (2009).
[24] R. K. Mondal, V. Chatterjee, S. Pal, Phys. E Low-Dimensional Syst. Nanostructures **108**, 233 (2018).
[25] S. Prasad, R. K. Mondal, V. Chatterjee, S. Pal, Superlattices Microstruct. **132**, 106167 (2019).
[26] R. K. Mondal, V. Chatterjee, S. Pal, IEEE Trans. Electron Devices **67**(4), 1674 (2020).
[27] R. K. Mondal, V. Chatterjee, S. Pal, Opt. Mater. **104**, 109846 (2020).
[28] R. K. Mondal, S. Adhikari, V. Chatterjee, S. Pal,

Mater. Res. Bull. **140**, 111258 (2021).

[29] Y. Li, S. Chen, W. Tian, Z. Wu, Y. Fang, J. Dai, C. Chen, IEEE Photonics J. **5**(4), 8200309 (2013).

[30] S. Das, T. R. Lenka, F. A. Talukdar, R. T. Velpula, B. Jain, H. P. T. Nguyen, G. Crupi, Eng. Res. Express **4**, 015030 (2022).

[31] S. Clara, Silvaco User's Manual Device Simulation Software, no. October, 2004, www.silvaco.com

[32] J. Yan, J. Wang, Y. Zhang, P. Cong, L. Sun, Y. Tian, C. Zhao, J. Li, J. Cryst. Growth **414**, 254 (2015).

[33] Y. P.Varshni, Physica **34**(1), 149 (1967).

[34] E. P. Coughlan, C. Schulz, S. Caro, M. A. O'Reilly, Phys. Stat. Solidi **252**, 879 (2015).

[35] J. Piprek, Nitride Semiconductor Devices: Principles and Simulation, Wiley Online Libr. Berlin, Ger. **590**, 2007.

[36] H. Hirayama, Recent Technol. Adv. **6**(4), 794 (2018).

[37] J. Yun, J. I. Shim, H. Hirayama, Appl. Phys. Express **8**(2), 022104 (2015).

[38] K. B. Nam, M. L. Nakarmi, J. Li, J. Y. Lin, H. X. Jiang, Appl. Phys. Lett. **83**(5), 878 (2003).

[39] D. M. Caughey, R. E. Thomas, Proc. IEEE **55**(12), 2192 (1967).

[40] S. Chuang C. Chang, Phys. Rev. B - Condens. Matter Mater. Phys. **54**(4), 2491 (1996).

[41] V. Fiorentini, F. Bernardini, O. Ambacher, Appl. Phys. Lett. **80**(7), 1204 (2002).

[42] Z. H. Zhang, S. T. Tan, Z. Ju, W. Liu, Y. Ji, Z. Kyaw, Y. Dikme, X. W. Sun, H. V. Demir, IEEE/OSA J. Disp. Technol. **9**(4), 226 (2013).

[43] I. Vurgaftman J. R. Meyer, J. Appl. Phys. **94**(6), 3675 (2003).

[44] J. K. Zettler, C. Hauswald, P. Corfdir, M. Musolino, L. Geelhaar, H. Riechert, O. Brandt, S. Fernández-Garrido, Cryst. Growth Des. **15**(8), 4104 (2015).

[45] H. P. T. Nguyen, S. Zhang, K. Cui, X. Han, S. Fathololoumi, M. Couillard, G. A. Botton, Z. Mi, Nano Lett. **11**(5), 1919 (2011).

[46] Z. H. Zhang, W. Liu, Z. Ju, S. Tiam Tan, Y. Ji, Z. Kyaw, X. Zhang, L. Wang, X. Wei Sun, H. Volkan Demir, Appl. Phys. Lett. **104**(24), 16 (2014).

_____

[*]Corresponding author: trlenka@ieee.org